Bollettino di Geofisica Teorica ed Applicata Vol. 62, n. 1, pp. 119-134; March 2021
DOI 10.4430/bgta0337

Discussion on monitoring and characterising group drilling pumping test within a massive thickness aquifer using the time-lapse transient electromagnetic method (TEM)

J. Zhang[1], K. Chen[2], H. Huang[2], L. Zhen[2], J. Ju[3] and S. Du[4]

[1] *School of Energy Resources, China University of Geosciences, Beijing, China*
[2] *State Key Laboratory of Simulation and Regulation of Water Cycle in River Basin, China Institute of Water Resources and Hydropower Research, Beijing, China*
[3] *Key Laboratory of Shale Gas and Geoengineering, Institute of Geology and Geophysics, Chinese Academy of Sciences, Beijing, China*
[4] *MLR Key Laboratory of Saline Lake Resources and Environments, Institute of Mineral Resources, Chinese Academy of Geological Sciences, Beijing, China*

(Received: 25 February 2020; accepted: 25 June 2020)

ABSTRACT To investigate underground hydrogeological conditions and to obtain accurate aquifer parameters, the time-lapse transient electromagnetic method (TEM) is applied to image groundwater drawdown within a massive thickness sandstone aquifer (thickness over 100 m) in Inner Mongolia, China. 2D geophysical models are established based on the hydrostratigraphy of the survey site and, then, the induced electromotive forces (EMF) pre- and post-pumping test are analysed. Multiple aquifers can be detected by 2D forward modelling and the unsaturated region can be distinguished by the variation of electromagnetic responses. Furthermore, the measured electromotive force curves before (pre-) and after (post-) pumping deviate from each other and the groundwater drawdown has a positive correlation with the deviation degree, namely relative variation. The raw EMF data are processed with Occam's inversion method and two 2D resistivity data volumes are obtained. The resistivity-depth cross-sections from the data volume show that the groundwater drawdown is larger in the east of the TEM area due to the large permeability and water content. The centre of the depression cone is located at east Pumping Well 1 and the drawdown is 70 m, which is basically coincident with the group drilling pumping test result.

Key words: time-lapse TEM, group drilling pumping, massive thickness aquifer, groundwater monitoring.

1. Introduction

As groundwater resources play an important role in sustainable water supplies, the needs of developing groundwater have been growing to provide clean water for communities. As the main method to investigate the water storage capacity of the aquifer, the pumping test is essential to assess water production capacity of a wellbore and to evaluate the exploitable amount of water source (Bear, 2013). The pumping test usually aimed at estimating hydrogeological parameters, analysing the relationship between the water inflow and the groundwater drawdown, and

determining the shape, size, and the growth rate of the depression cone. Currently, results-based estimates of hydrogeological parameters have been implemented mainly by both classical methods and homogeneous-interpretation models (Theis, 1935; Cooper and Jacob, 1946). However, time-varying hydrogeological parameters in test evaluations may be driven by the unsteady cone of depression associated with heterogeneous aquifers (Leven and Dietrich, 2006). Therefore, it is important to monitor this time-varying geometry and understand the actual groundwater distribution after pumping (Chang *et al*., 2017). Unfortunately, the knowledge on identifying the time-varying geometry and physical properties in the subsurface is a contemporary challenge for most researchers, in particular for groundwater and its protection from contamination (Garambois *et al*., 2002; Hatherly, 2013).

In addition, drilling a series of wells for the specific purpose of monitoring is time-consuming as well as uneconomical, especially for those massive thickness aquifers. As a result of relative low pumping capacity, single-well pumping is seldom applied in thick aquifers. This is because a large drawdown usually could not be obtained by single-well pumping due to the rapid recharge from surrounding groundwater. Thus, we could not accurately analyse the relationship between groundwater inflow and its drawdown. Owing to larger pumping capacity, group drilling pumping is a better choice for a massive thickness aquifer, which also means more peripheral observation wells and more complex groundwater immigration.

Aware of these issues, researchers have focused their eyes on non-invasive geophysical methods for monitoring underground aquifers, such as ground-penetrating radar [GPR; Bevan *et al*. (2003)], self-potential (SP) method (Titov *et al*., 2005), and electrical resistivity tomography [ERT; Toran *et al*. (2010); Chang *et al*. (2017)]. Former studies show that it is a wise choice to use the geoelectric parameters to characterise the hydrogeological conditions. For one thing, it was demonstrated that the resistivity decreases as a negative power function with the water volume increases (Liu *et al*., 2010). On this basis, establishing the quantitative electrical-hydraulic relations helps us to improve our understanding of spatially-distributed aquifer properties (Ikard and Krewss, 2016), to define the spatial location of the water-containing goaf (Xue *et al*., 2013; Yang *et al*., 2017; Chen *et al*., 2019a) or to estimate the water bursting volume. For another thing, the resistivity visualisation technology was proposed to realise dynamic monitoring of the groundwater movements. A similar methodology of electrography, that detects piezometric head distribution during pumping tests by the electrical responses, allows to visualise preferential fluid flow pathways and the distribution of heads (Rizzo *et al*., 2004).

The electromagnetic method is a high-precision and low-cost geophysical method, which has great advantages in low-resistivity body recognition and has a wide application prospect with the development of 3D forward modelling and joint inversion methods (Key, 2009, 2016; Li *et al*., 2018, 2019). A time-lapse transient electromagnetic method (TEM) collects the electromagnetic data at different times at survey points of high density and, then, monitors the spatial and temporal changes for the subsurface target (Berre *et al*., 2011; Girard *et al*., 2011). Compared with the Direct Current (DC) resistivity method, the time-lapse TEM provides better delineation of the hydrogeological characteristics of aquifers in a nonintrusive cost-effective and high efficient way by a better vertical resolution (Robinson *et al*., 2008; Chen *et al*., 2019b). To date, most of the researches on the time-lapse TEM have focused on monitoring oil and gas reservoirs (Lien and Mannseth, 2008). For instance, the time-lapse marine controlled-source electromagnetic method (CSEM) with 2D reservoir-depletion modelling was applied for monitoring a resistive hydrocarbon

reservoir. Orange *et al*. (2009) found a measurable change in the CSEM response when 10% of a reservoir was replaced by conductive pore fluids. He *et al*. (2012) monitored hydraulic fracturing using audio-frequency magnetotellurics in shale gas reservoirs. However, few studies have led to accurately monitor and characterise groundwater drawdown under complex pumping conditions.

In this paper, we explore characterising groundwater movement within the massive thickness sandstone aquifer based on a time-lapse TEM monitoring operation at an experimental area of Inner Mongolia, China. First, group drilling pumping test is conducted and the basic hydrogeological parameters are obtained. Then, according to the hydrogeological condition of the survey area and the distribution of the groundwater pre- and post- pumping test, we construct 2D geophysical models and discuss characteristics of electromagnetic responses observed on the surface. Third, the field experiment process of the time-lapse TEM is introduced, and the measured data are analysed and processed in detail. Finally, we analyse the changes of electromagnetic responses caused by pumping activities and compare the actual effect of time-lapse TEM with that of group drilling pumping test.

2. Survey backgrounds

The survey area is situated in the south-western part of Hulun Buir, Inner Mongolia, China (Fig. 1a), which has a typical low hilly topography (Fig. 1b). Argun River, Wuerxun River, and Yimin River flow through the survey area. The survey site is adjacent to the east of Yimin River and the terrain is relatively flat. Stratigraphic development of the survey area includes a bottom-up composition of Cretaceous and Quaternary (Fig. 1c). The Coal seam 15-1 is stably and continuously developed in the lower part of the Yimin Formation, Cretaceous, which is the marker layer of the survey area.

Hydrostratigraphy is relatively simple in the survey area. Two isolate aquifers are certified in this study, including the Quaternary (Q) aquifer (near surface) and the Yimin aquifer (above Coal seam 15-1). The Q aquifer is regarded as a phreatic aquifer, which consists of Q unconsolidated conglomerate rocks. The drilling and well-logging data show that the Q aquifer has an average thickness of 11 m, permeability coefficient (K) of 0.0015-0.6100 m/d and unit water inflow (q) of 0.0004-0.0400 L/s·m. The Yimin aquifer mainly consists of medium-coarse sandstone, with some thin mud layers. Compared with the Q aquifer, the Yimin aquifer has a larger thickness of 133 m and richer water abundance (K = 0.231-8.239 m/d and q = 0.05-2.47 L/s·m), and, therefore, this aquifer is selected as the survey target in this study. Meanwhile, there are two separate aquitards with poor water abundance: Q aquitard, and the coal seam aquitard. Q aquitard consists of Q clays and silty clays, and the coal seam aquitard contains the Cretaceous coal rocks, sandstone and muddy sandstone. Moreover, these two aquitards play as good water barriers because they are so continuously developed that the groundwater cannot be able to flow across the aquifers vertically.

3. Feasibility analyses

Previous studies have verified the feasibility of TEM application in detecting multiple aquifers using 1D or 2D forward models (Yan *et al*., 2016; Xue *et al*., 2018; Chen *et al*., 2019b). For two

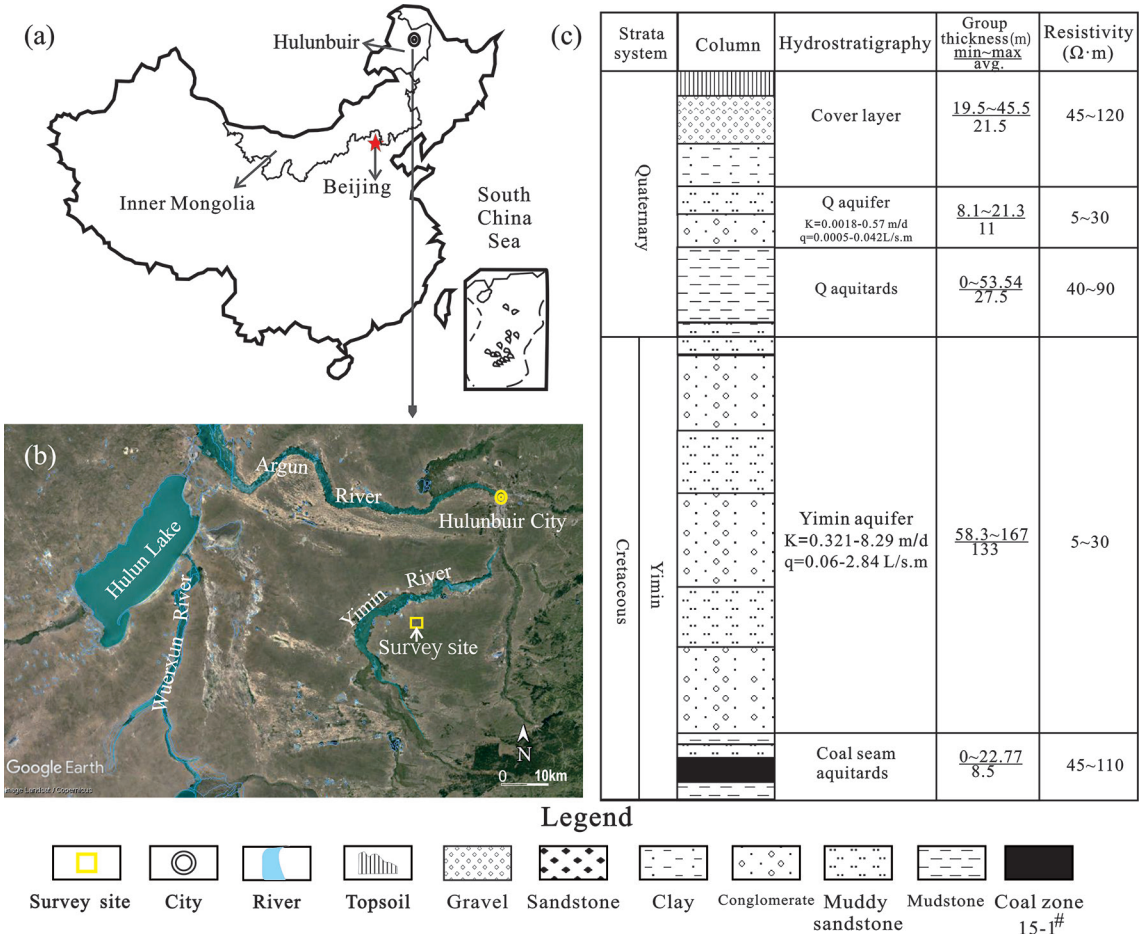

Fig. 1 - Location of the survey site and hydrostratigraphy of the survey area: a) location of the survey area; b) location of the survey site; and c) vertical hydrogeology of the survey area.
Note: resistivity was obtained from previous well logging data.

separate aquifers that exist in a survey area, three 2D models were constructed to examine the variation in the induced electromotive force (EMF, the unit is $V \cdot m^{-2}$) observed on the Earth's surface at pre- and post- pumping test. The geophysical models of the survey site are detailed in Fig. 2.

The 2D forward model consists vertically of 5 layers, which is consistent with the hydrostratigraphy of the survey area (Fig. 1c). Geophysically, the Q aquifer and the Yimin aquifer are relatively low-resistivity layers while the Q aquitard and the coal seam aquitard are relatively high-resistivity layers. The main features of the three 2D geophysical models established in this study are as follows:

- Model 1 is a reference model that is a single aquifer with resistivity $\rho_1 = \rho_3 = \rho_4 = \rho_5 = 150$ ohm·m and $\rho_2 = 15$ ohm·m (Fig. 2a);
- Model 2 was established to represent the condition of pre-pumping, i.e. the actual hydrogeology that consists of two saturated aquifers with $\rho_1 = \rho_3 = \rho_5 = 150$ ohm·m and $\rho_2 = \rho_4 = 15$ ohm·m (Fig. 2b);
- Model 3 represents the condition of post- pumping.

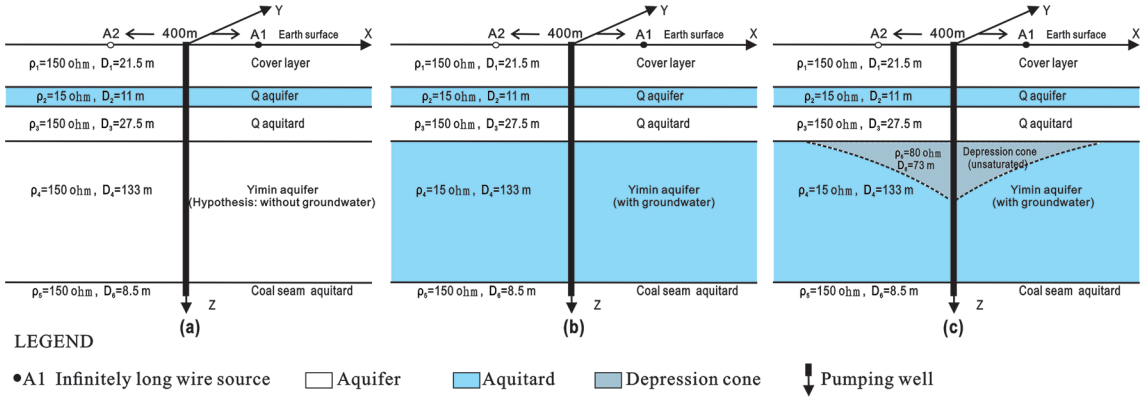

Fig. 2 - 2D geophysical models of the aquifers, the aquitards and the depression cone based on the geological and hydrogeological condition in the survey area.

An unsaturated zone, in the form of a groundwater depression cone, appears in the Yimin aquifer with $\rho_1 = \rho_3 = \rho_5 = 150$ ohm·m, $\rho_2 = \rho_4 = 15$ ohm·m, and $\rho_6 = 80$ ohm·m (ρ_6 is in the region of the depression cone). The influence radius of the groundwater depression cone and the maximum groundwater drawdown were set to 1000 and 73 m, respectively (Fig. 2c).

In addition, the transmitter loop size is 360×360 m^2, transmitting current is 10 A, and the receiver position is on the centre-line of the transmitter loop. The emission source includes two parallel infinitely long wire sources along with different directions (A1 and A2, as shown in Fig. 2) for the current (Oristaglio, 1982). A1 and A2 were placed at -200 and at 200 m, respectively. The changes of EMF observed on the Earth's surface pre- and post- pumping will be analysed and the pumping hole was arranged at the original position. The finite difference time domain method (FDTD) was adopted to calculate the 2D forward modelling of models 1 to 3 (Oristaglio and Hohmann, 1984; Yan *et al*., 2002). Furthermore, the vertical EMF in the range of -200 to 200 m along with an X-direction was calculated.

The results of the 2D forward model were shown in the EMF decay curves (Fig. 3). Obviously, the three EMF decay curves have a large separation driven by the heterogeneity of geophysical

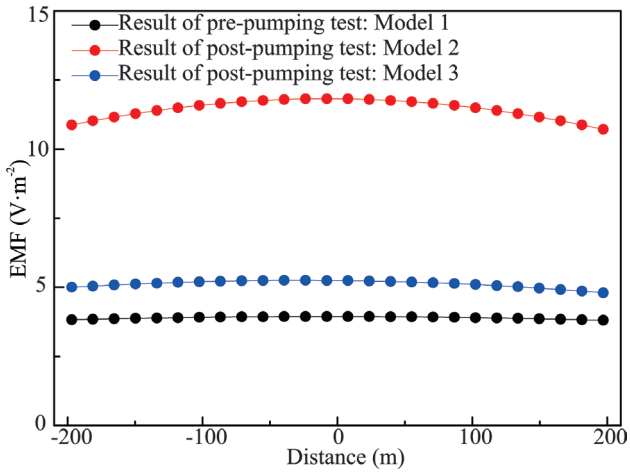

Fig. 3 - 2D forward modelling results: decay curves of the induced electromotive force.

characteristics. Firstly, the EMF value of Model 1 ranges from 3.80 to 3.94 Vm^{-2}, which is significantly higher than that of Model 2 (from 10.71 to 10.82 Vm^{-2}). Such a result indicates that changes in the observed signals may be caused by groundwater distributions and, consequently, TEM can be a proper alternative to detect a thick aquifer (e.g. Yimin aquifer), especially for an overlaying thin aquifer (e.g. Q aquifer). Secondly, the results of Model 2 showed that the Q aquifer and the Yimin aquifer were remaining in an initial state. Assuming that these two aquifers are saturated, such a result indicates that there is no hydraulic connection between them under the condition of pre- pumping. Model 3 simulation showed that water level in the Yimin aquifer and the water abundance decreased, while the resistivity nearby the groundwater depression cone increased. During the whole pumping processes, the Q aquifer remained unchanged and, meanwhile, the Yimin aquifer did not obtain groundwater recharge from the Q aquifer. Compared to Model 2, the EMF values of Model 3 decreased by a range of 4.79 to 5.24 $V \cdot m^{-2}$, indicating a decrease in the water content and saturation of the Yimin aquifer. Fig. 4 shows the relative variation in EMF values (d) between two 2D models as shown in Eq. 1:

$$\delta = \frac{\left| R_{model0} - R_{model} \right|}{R_{model0}} \tag{1}$$

where R_{model0} and R_{model} are two different EMF values.

The relative variations simulated in this study were greater than 30% in the whole range of the loop, 64.49 to 66.67% between Model 1 and Model 2, while 55.21 to 55.63% between Model 2 and Model 3. Previous studies suggested that the two low-resistivity layers can be distinguished in the case that the relative variation is greater than 30% (Niu, 2007; Yan *et al*., 2016; Xue *et al*., 2018). Therefore, these results demonstrate that two aquifers can be detected without hydraulic connection and pumping activities may induce a larger variation of responses between pre- and post- pumping.

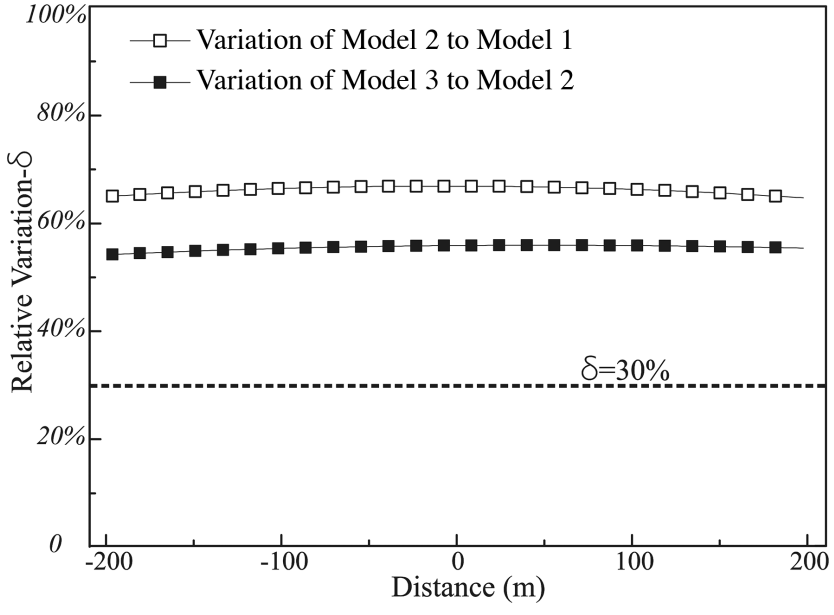

Fig. 4 - Relative variation of two 2D forward models: 2 to 1: 64.49-66.67%; 3 to 2: 55.21-55.63%.

4. Data acquisition and processing

In order to evaluate the feasibility of using time-lapse TEM to monitor the groundwater movement in the sandstone aquifer, group drilling pumping test and time-lapse TEM were carried out, respectively, in the survey site (Fig. 1b; see Fig. 5 for the work flow chart). The time-lapse TEM field tests were carried out twice around the pumping well group (Fig. 6a).

4.1. Layout of the survey site

The survey site consists of a pumping well group and observation wells. Well 1, Well 2, Well 3, and Well 4 denote pumping wells in a pumping well group (Fig. 6a). These four pumping

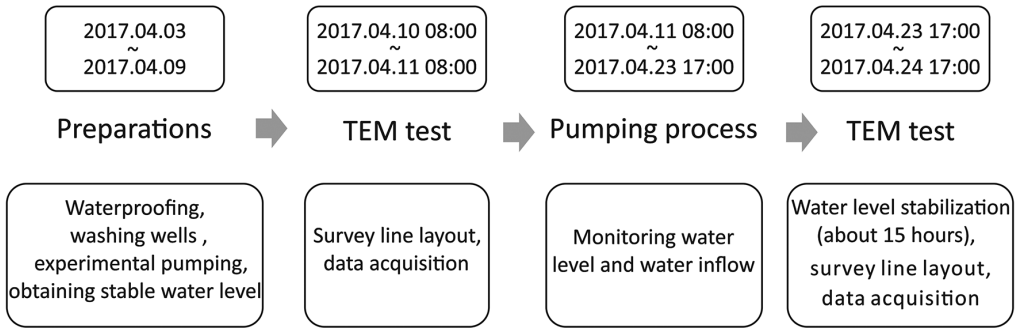

Fig. 5 - Time steps for the group drilling pumping and TEM test.

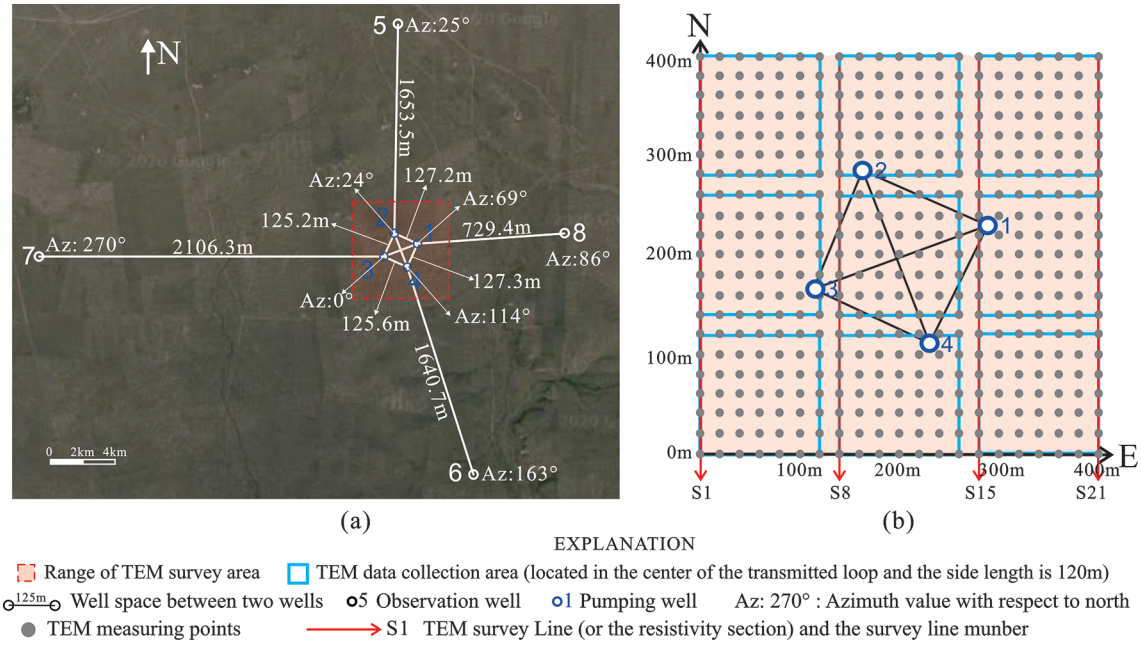

Fig. 6 - Layout of the pumping test and the time-lapse TEM in the survey site: a) location of the pumping well groups and the observation wells; b) location of the TEM survey points and the TEM survey lines and the relative position of the pumping well group in the TEM survey area.

wells were placed in the form of a square well pattern, spacing at 127 m between two adjacent well holes. The pumping well group is surrounded by four peripheral observation wells, i.e. Well 5, Well 6, Well 7, and Well 8. The distance between one observation well and the pumping well group centre ranged from 729 to 2106 m to ensure that the whole survey site is large enough to conduct a hydrogeological and geophysical exploration.

4.2. Group drilling pumping test

Four submersible pumps with the capacity of 180 m^3/h were employed into the four pumping well holes for the Yimin aquifer, the target pumping layer. Prior to the pumping test, waterproofing, washing wells, and experimental pumping were implemented. In addition, the water level in the hole was restored to the approximate static water level to meet the stability standard. Then, pumping water was conducted for 297 hours. An electronic water level gauge was applied to measure the water level. Furthermore, a water-flowmeter and a triangular weir were used together for measuring water flow. In the meantime, the four peripheral observation wells also monitored the groundwater variation once a day. After pumping, a stabilisation process (about 15 hours) was implemented not only to measure the stabilised water level in each well hole after pumping, but also to catch more reliable consequences and corresponding insights for water drawdown. The final pumping results are presented in Table 1.

Table 1 - Hydrogeological Yimin aquifer and pumping test results.

Well name	Yimin Aquifer (m)	Static water level (m)	Water drawdown (m)	Water inflow ($Q/L \cdot s^{-1}$)	Unit water inflow ($q/L \cdot (s \cdot m)^{-1}$)	Permeability coefficient (m/d)
1	55.9-202.1	660.6	73.2	107.5	1.469	4.3
2	62.1-199.3	660.3	46.5	47.4	1.019	2.1
3	62.4-202.0	660.7	46.6	44.4	0.953	1.9
4	62.6-197.0	658.5	45.2	44.1	0.976	2.1
5	61.7-192.0	661.2	2.7	-	-	
6	61.5-198.2	668.6	3.2	-	-	
7	62.3-199.1	655.7	0.3	-	-	
8	61.3-201.6	666.8	1.3	-	-	

4.3. TEM survey (data acquisition)

The survey lines of the time-lapse TEM area were comprised of 20 (line distance) × 20 m (dot pitch) and 441 survey points overall, along with the N-S direction as shown in Fig. 6b. In this measurement, a V8 multi-function electromagnetic instrument was used to receive the induced voltage, which covers the receiving area of 100 m^2. The specific parameters of TEM measurement are:

1) a large loop device;
2) transmitter loop size (360×360 m^2);
3) time window from 0.1 to 47.5 minutes;
4) fundamental frequency (5 Hz);
5) transmitted current (10.0±0.5 A);

6) observation time (2~3 minutes);
7) delay time (100 μs);
8) number of gates (40);
9) stacking (2667).

Two transient electromagnetic measurements were performed in this survey: one measured the electromagnetic responses that represent the initial groundwater state before pumping water; the other measured the electromagnetic response under the maximum drawdown of the groundwater once the water level is steady in the pumping well hole after the pumping test. Both measurements were accomplished within 24 hours to ensure the authenticity and validity of the data and the measurements were repeated at least 3 times at the same location.

4.4. Data processing

Processing the raw data measured in the field is an essential part of the geophysical technique for improving the quality of results. Noises from various sources were removed from all the raw data in order to retrieve more reliable observations. Due to the characteristics of a wide frequency band and fast attenuation of the TEM signal, a smoothing technique needs to be conducted for the decay curve of one measurement point. This study applied a human-computer interaction technique, based on a self-designed program (Li *et al.,* 2016b), which mainly consists of two steps: first, removing sharp points and second, replacing outliers (i.e. high fluctuation and high dispersion points) with the average value of the adjacent data. Specifically, Occam's inversion method with constraint conditions (Constable *et al*., 1987; Li *et al*., 2015) was used. The objective function for the inversion is (Li *et al*., 2016a):

$$\min\left\{ \left\| WF(m^k) + WJ(m^k)\,\Delta m - Wd \right\|_2^2 - x_0{}^2 \right\} + \alpha^2 \left\| L(m^k + \Delta m) \right\|_2^2 \tag{2}$$

where: F is the forward operator, J is the Jacobian matrix, d is the data vector, x_0 is the target misfit value, and α is the Lagrange multiplier, which is used to balance the misfit and the roughness term. L is the roughness matrix to implement the Tikhonov regularisation. W is the data weighting matrix to incorporate the standard deviations:

$$W = \mathrm{diag}\left(\sigma_1^{-1}, \sigma_2^{-1}, \cdots \sigma_M^{-1} \right) \tag{3}$$

where the σ_1 represents an estimation of the error in the data. By minimising the defined objective function (Eq. 2), the smoothest resistivity model for a given target misfit can be obtained. To minimise Eq. 2 with respect to the model vector m^k, and let:

$$d(m^k) = d - F(m^k) + J(m^k)m^k\,. \tag{4}$$

Then, the iterative solution can be found using the Gauss-Newton method,

$$m^{k+1} = m^k + \Delta m = \left(J(m^k)^T J(m^k) + \partial^2 L^T L \right)^{-1} (J(m^k)^T d(m^k) \tag{5}$$

5. Results and analyses

5.1. Pumping test results

As illustrated in Fig. 7, the terrain slopes gently and the initial groundwater level maintains between 655.7 and 668.8 m in the whole survey site. Both the topography and water level are slightly higher in the east and south. As the initial groundwater levels were similar to each other over the TEM area, the pumping test could hardly be affected by the groundwater dynamics. After pumping, the groundwater level dropped generally in the survey site and the cone of depression occurred inside the pumping well group. The peripheral groundwater drawdowns for the north Well 5, south Well 6, west Well 7, and east Well 8 were 2.7, 3.2, 0.3, and 1.3 m, respectively. Such a result indicates that the influence radiuses of depression cone to the north, south, west, and east are over 1653.5, 1640.7, 2106.3, and 729.4 m, respectively. Moreover, it is noteworthy that the groundwater drawdown varied with the range of the TEM area. The deepest drawdown occurred in Well 1 (73.2 m) that may lead to the irregular depression cone, compared to other wells (Well 2 of 45.2 m, Well 3 of 46.6 m and Well 4 of 46.5 m). The depression cone is relatively smooth and symmetrical in the N-S direction (Fig. 7a) while the depression cone was asymmetrical and sharp in the east (Fig. 7b). These results can be explained by the lateral variation of the water-bearing property across the TEM area, regardless of groundwater recharge and loss, or pumping equipment and capacity. In other words, the permeability of the aquifer in the east part of the TEM area (or within the range of Pumping Well 1) was higher than other parts as shown in Table 1, which illustrates that the permeability coefficient (4.3 m/d) and the unit water inflow [1.469 q/L·(s·m)$^{-1}$] for Well 1 were higher than those for other pumping wells.

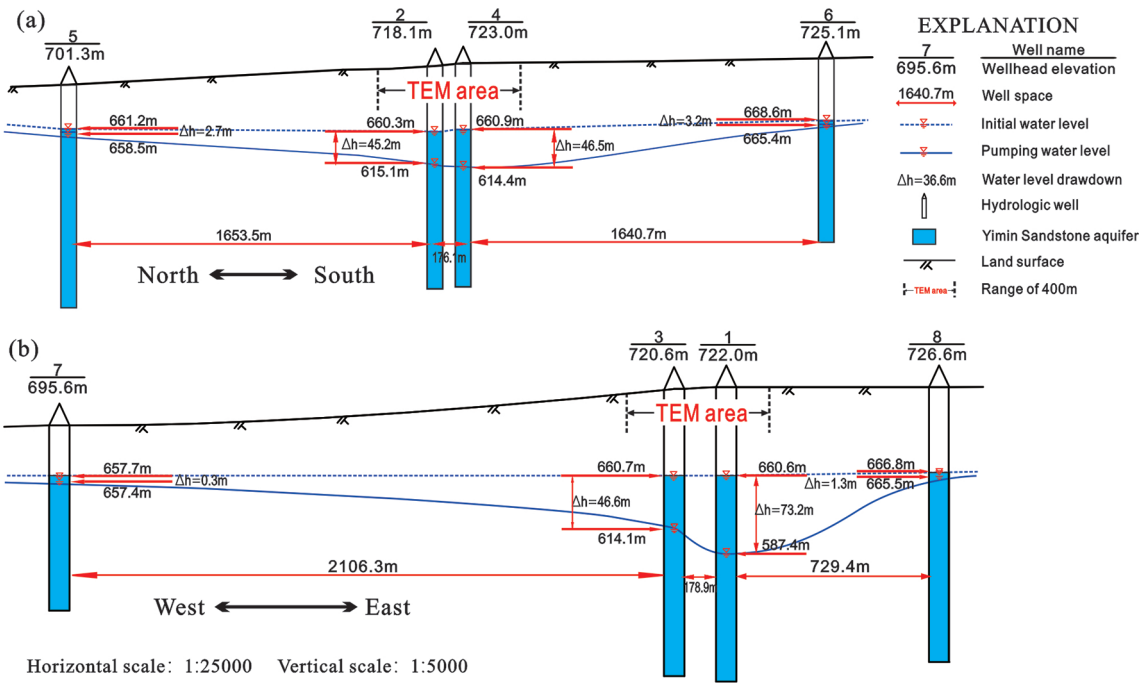

Fig. 7 - Hydrogeological profiles for the groundwater level changes pre- and post-pumping based on pumping test result in the whole survey site: a) N-S profile; b) E-W profile. For well location see Fig. 5a.

5.2. TEM results

As mentioned in 2D forward modelling results, noticeable variations in electromagnetic responses can be observed when the groundwater distribution is changed. During this geophysical investigation, the raw data of measured electromotive force under the conditions of pre- and post-pumping were collected respectively at the 441 coordinate points in the survey site. However, the pumping process caused an unneglectable disturbance around the pumping well hole in the late time. Therefore, this study first removed the effect of the pumping process to avoid unexpected biases in measurements, and, then, the relative variations of measured electromotive force pre- and post- pumping were calculated. The characteristic instances presented in the double Y coordinate system (Fig. 8).

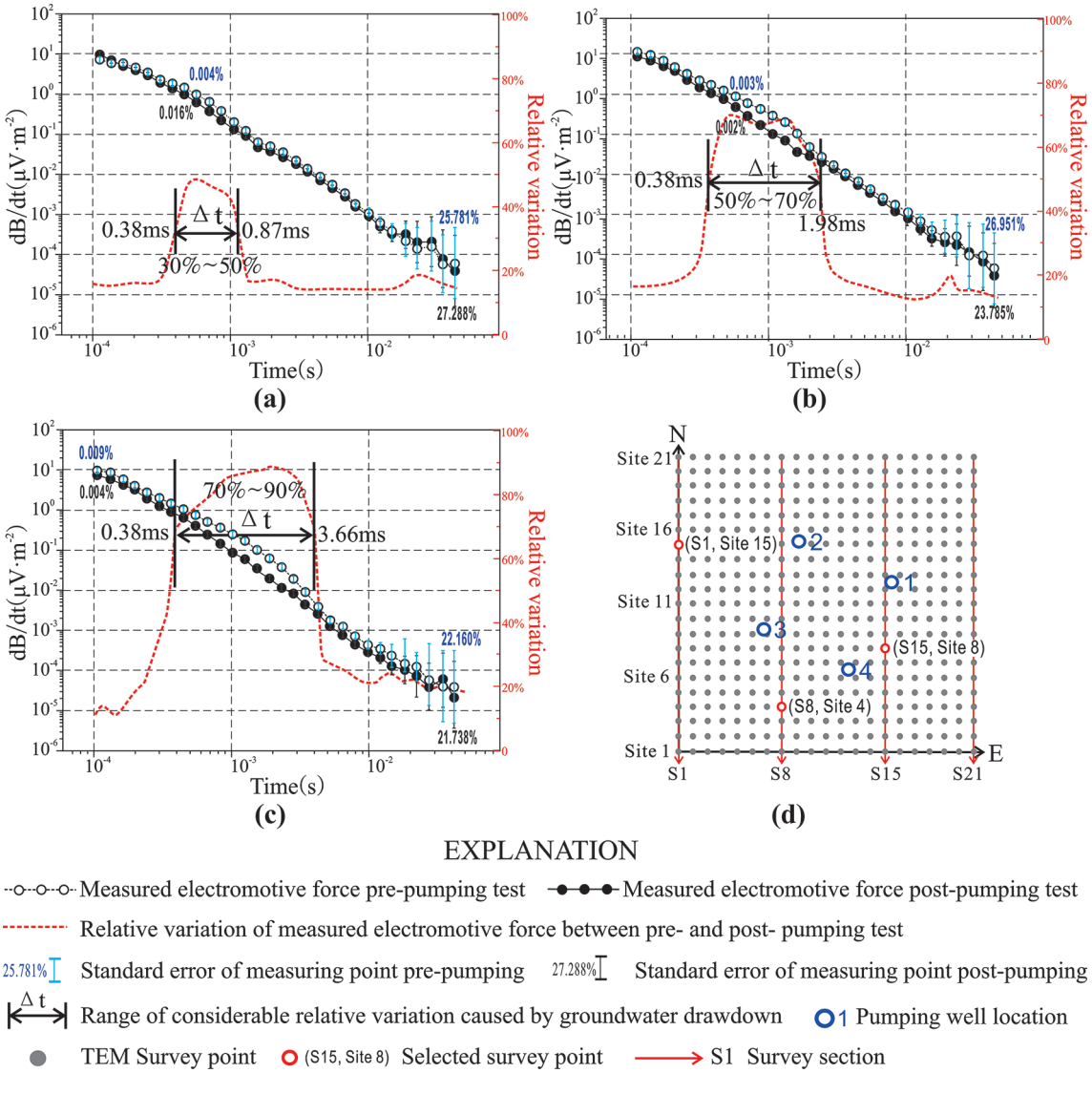

Fig. 8 - Measured electromotive force and relative variation of the selected points pre- and post-pumping: a) Line S1 site 15; b) Line S8 site 4; c) Line S15 site 8; d) location of the selected survey points.
Note: maximum and minimum value of the standard error of survey point are labeled beside the error bars.

Compared with the pre-pumping situation, it is prominent that the measured electromotive forces at each coordinate point under the post-pumping condition exhibited relatively lower in the mass. This is caused by a decrease in the water abundance of the underground aquifer and an increase in the resistivity. Moreover, the measured electromotive force curves for the pre- and post- pumping deviated from each other at varying degrees from different coordinate points. The relative variation curves showed approximately a parabolic pattern. At Site 15 of Line S1 (Fig. 8a) for example, considerable discrepancy occurred at the time inflection point of the relative variation curve (0.38 ms) and disappeared at another time inflection point (0.87 ms). These two time inflection points were defined as a time slot (Δt) that represents the range of a considerable deviation. Three typical types for the relative variations were identified: slight variations with δ = 30-50% at Site 15 of Line S1 (Fig. 8a); moderate variations with δ = 50-70% at Site 4 of Line S8 (Fig. 8b); and significant variations with δ = 70-90% at Site 8 of Line S15 (Fig. 8c). The corresponding Δt are 0.38-0.87, 0.38-1.98, 0.38-3.66 ms, respectively, and showed a positive correlation with the relative variation.

It was found that all the measured electromotive force curves for the pre- and post-pumping were similar to each other initially, considerable deviations appeared over time, and, then, the curves were turned to a steady-state again with small fluctuations in the end. Employing the Occam inversion method, the responses of the three selected coordinate points mentioned in Fig. 8 are processed to better explain the meaning of actual geological characteristics. Fig. 9 shows the 1D inversion Occam's results. Through the inversion process, the measured electromotive forces and time were converted to resistivity and burial depth, respectively, and subsequently, the inversion curve became just the resistivity curve. There were two obvious low-resistivity layers, the Q aquifer (burial depth: 30-40 m) and the Yimin aquifer (burial depth: 60-190 m). When the variation of the induced electromotive forces between pre- and post- pumping is less than 30%, there should be little change in the resistivity curve. In other words, the resistivity curves for pre- and post- pumping were almost coincident except for the upper part of the Yimin aquifer where the considerable deviations of the relative variation curves existed (Fig. 8). However, there was

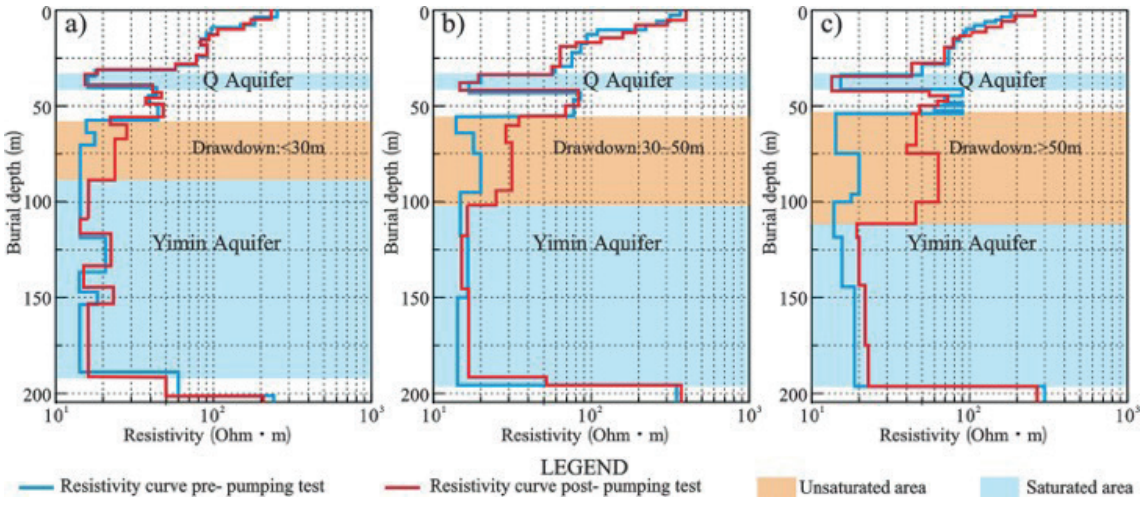

Fig. 9 - 1D Occam's inversion results of the measured points pre- and post-pumping: a) Line S1 site 15; b) Line S8 site 4; c) Line S15 site 8.

little offset between the resistivity curves between pre- and post- pumping at the depth of the Q aquifer, indicating that the groundwater of the Q aquifer remains in its original state throughout the pumping process. In Fig. 9a, the resistivity value for the post-pumping in the Yimin aquifer was nearly doubled than that for pre-pumping at a certain range of depth (50-85 m), which is mainly driven by a decrease in the groundwater drawdown (<30 m). In Figs. 9b and 9c, the resistivity of the post-pumping increased by 2-5 times as the groundwater drawdown increased by 30-50 m and above 50 m. Therefore, the water level changes can be detected by the electrical anomaly area on the resistivity curve.

Next, two 2D resistivity data volumes for pre- and post-pumping were successively obtained, which are a reflection of the stratigraphic and water-bearing conditions underground. The resistivity-depth cross-sections of the four lines (Line S1, Line S8, Line S15, and Line S21) in the survey site (Figs. 6b and 8d) were evenly selected and they were given in a vertical arrangement in Fig. 10. Figs. 10a and 10d show the resistivity contour maps for the pre- pumping while those of the post- pumping are shown in Figs. 10e to 10h, where the blue and red areas represent low and high resistivity. In the contour maps for the pre- pumping, five strata were identified in the vertical direction, which is consistent with the geological information from drilling. The resistivity gradually moved from blue to red. Two distinct low-resistivity layers at the depth of 30-40 m and 60-200 m corresponded to the Q aquifer and the Yimin aquifer, respectively. The Q aquitard is a continuous layer with a high resistivity, which effectively prevents potential watercourses between the two aquifers. The coal seam aquitard at the bottom is a good floor to resist water, resulting in preventing water leakage. Then, the four pumping wells 1 to 4 are projected on the cross-sections, as a scale of water level change in the pumping process of group wells.

The final inversion results show that a significant change in the resistivity of the post-pumping was detected in the Yimin aquifer, which may be driven by the groundwater drawdown. It is noted that the pumping well group is located in the centre part of the TEM survey area and survey sections S1, S8, S15, and S21 are arranged in order from the west to east. Therefore, different electrical resistivity characteristics may be obtained from different survey sections. Survey Section S1 (Figs. 10a to 10e) is situated at the westernmost side of the survey site and is relatively far away from the pumping group centre, as shown in Fig. 8d. The burial depth of the initial water level in the Yimin aquifer was around -60 m while the water level decreased by -85 m after pumping. The water level was nearly a horizontal line and the groundwater drawdown was about 25 m. Survey Section S8 close to Well 2 and Well 3 (Figs. 10b to 10f) passed through the pumping group. Seen from Fig. 10f, the water level of the post-pumping showed a gentle arc shape with higher values at far ends and the lowest value in the middle. The largest groundwater drawdown (45 m) occurred between Well 2 and Well 4, which is a reasonable depth reduction driven by the depression cone in the centre of the well group according to the pumping test (Fig. 7 and Table 1). Survey Section S15 close to Well 1 and Well 4 (Figs. 10c and 10g) is another profile across the group centre. Due to the large pumping volume and the groundwater drawdown of Well 1, a clear cone-shaped unsaturated zone appeared in the Yimin aquifer (Fig. 10g). The groundwater drawdown increased by 40 m on both sides and the maximum drawdown occurred at Well 1 (about 70 m), which is similar to the drawdown of Well 1 (73.5 m) from the pumping test. In the easternmost Survey Section S21 (Figs. 10d and 10h) distributed symmetrically with S1, the water level of the post-pumping was slightly inclined. The groundwater drawdown was 27 m in

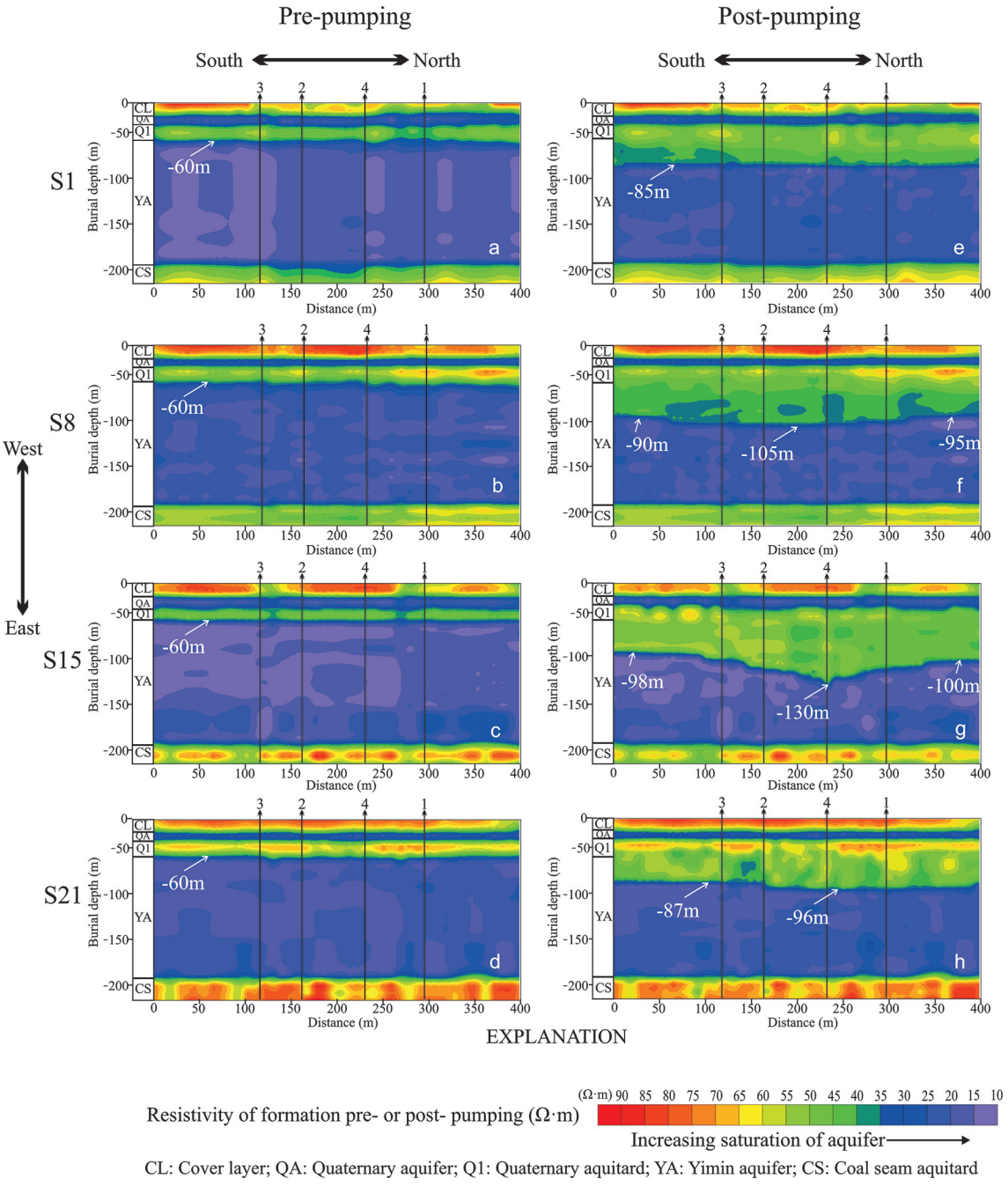

Fig. 10 - Resistivity-depth cross-sections. Cross-sections S1 to S21 are placed from west to east; the left-to-right direction in each cross section is equal to south-to-north direction in Fig. 5b.

the south and increased by 36 m to the north, which means that the northern part is considerably influenced by Well 1 (Fig. 10h). In brief, in the range of TEM survey area, the groundwater water levels in the west were higher than those in the east and the centre of the depression cone was located at Well 1, which is consistent with the pumping test.

6. Conclusions

On the basis of group drilling pumping test and numerical simulations, a feasibility investigation on the time-lapse TEM has been carried out to monitor the groundwater drawdown within a massive thickness sandstone aquifer. The results showed:

1) the 2D forward modelling results showed that EMF on the surface was obviously weakened after pumping and the electromagnetic variation in the unsaturated region of the aquifer was distinguished. Therefore, the time-lapse TEM could be applied to monitor groundwater depletion;
2) the relative variation of the measured electromotive forces between pre- and post- pumping showed a positive correlation with the groundwater drawdown, indicating that it is possible to characterise the groundwater distribution after pumping;
3) the TEM data obtained from the pre- and post-pumping within a study area of 1600 m^2 were processed and stored in a 2D data volume. The survey section of the data volume showed that the groundwater level decreased by 25-70 m in the detective area, and an asymmetrical depression cone was formed in the pumping process, which may be caused by the various permeability of the aquifers.

In general, the time-lapse TEM is an effective and intuitive method to monitor and depict the groundwater depletion in the sandstone aquifers.

Acknowledgements. The authors wish to thank the reviewers' efforts and their valuable suggestions. This research was supported by the National Key R&D Program of China (2018YFC0407102), the Natural Science Foundation of China (41474095, 41874162), the IWHR Basic Research Fund (SM0145B252020), and the Beijing Natural Science Foundation (8182054)..

REFERENCES

Bear J.; 2013: *Dynamics of fluids in porous media*. Courier Corporation, Honolulu, HI, USA, 764 pp.

Berre I., Lien M. and Mannseth T.; 2011: *Identification of three-dimensional electric conductivity changes from time-lapse electromagnetic observations*. J. Comput. Phys., **230**, 3915-3928.

Bevan M.J., Endres A.L., Rudolph D.L. and Parkin G.; 2003: *The non-invasive characterization of pumping-induced dewatering using ground penetrating radar*. J. Hydrol., **218**, 55-69.

Chang P.Y., Chang L.C. and Hsu S.Y.; 2017: *Estimating the hydrogeological parameters of an unconfined aquifer with the time-lapse resistivity-imaging method during pumping tests: case studies at the Pengtsuo and Dajou sites, Taiwan*. J. Appl. Geophys., **144**, 134-143.

Chen K., Xue G.Q. and Chen W.Y.; 2019a: *Fine and quantitative evaluations of the water volumes in an aquifer above the coal seam roof, based on TEM*. Mine Water Environ., **38**, 49-59, doi: 10.1007/s10230-018-00573-2.

Chen K., Zhang J.Y. and Xue G.Q.; 2019b: *Feasibility of monitoring hydraulic connections between aquifers using time-lapse TEM: a case history in Inner Mongolia, China*. J. Environ. Eng. Geophys., **24**, 361-372.

Constable S.C., Parker R.L. and Constable C.G.; 1987: *Occam's inversion: a practical algorithm for generating sooth models from electromagnetic sounding data*. Geophys., **52**, 289-300.

Cooper H.H. and Jacob C.E.; 1946: *A generalized graphical method for evaluating formation constants and summarizing well field history*. Trans. Am. Geophys. Union, **27**, 526-534.

Garambois S., Sénéchal P. and Perroud H.; 2002: *On the use of combined geophysical methods to assess water content and water conductivity of near-surface formations*. J. Hydrol., **259**, 32-48.

Girard J.F., Coppo N., Rohmer J., Bourgeois B., Naudet V. and Schmidt-Hattenberger C.; 2011: *Time-lapse CSEM monitoring of the Ketzin (Germany) CO_2 injection using 23 MAM configuration*. Energy Procedia, **4**, 3322-3329.

Hatherly P.; 2013: *Overview on the application of geophysics in coal mining*. Int. J. Coal Geol., **114**, 74-84.

He L., Hu X., Xu L., He Z. and Li W.; 2012: *Feasibility of monitoring hydraulic fracturing using time–lapse audiomagnetotellurics*. Geophys., **77**, 119-126.

Ikard S.J. and Kress W.; 2016: *Electric-hydraulic correlations in layered aquifers: a case study of the surficial aquifer of Emirate Abu Dhabi, United Arab Emirates*. J. Environ. Eng. Geophys., **21**, 187-200.

Key K.; 2009: *1D inversion of multicomponent, multifrequency marine CSEM data: methodology and synthetic studies for resolving thin resistive layers*. Geophys., **74**, 1MA-Z35.

Key K.; 2016: *MARE2DEM: a 2-d inversion code for controlled-source electromagnetic and magnetotelluric data*. Geophys. J. Int., **207**, 571-588.

Leven C. and Dietrich P.; 2006: *What information can we get from pumping tests? Comparing pumping test configurations using sensitivity coefficients*. J. Hydrol., **319**, 199-215.

Li G., Li Y., Han B. and Liu Z.; 2018: *Application of the perfectly matched layer in 3D marine controlled-source electromagnetic modelling*. Geophys. J. Int., **212**, 333-344.

Li G., Cai H. and Li C.F.; 2019: *Alternating joint inversion of controlled-source electromagnetic and seismic data using the joint total variation constraint*. IEEE Trans. Geosci. Remote Sens., **57**, 5914-5922, doi: 10.1109/TGRS.2019.2903043.

Li H., Xue G.Q., Zhou N.N. and Chen W.Y.; 2015: *Appraisal of an array TEM method in detecting a mined-out area beneath a conductive layer*. Pure Appl. Geophys., **172**, 2917-2929.

Li H., Xue G.Q. and Zhao P.; 2016a: *Inversion of arbitrary segmented loop source TEM data over a layered earth*. J. Appl. Geophys., **128**, 87-95.

Li H., Xue G.Q., Zhao P., Zhong H.S. and Khan M.Y.; 2016b: *The Hilbert - Huang transform based refining method for the TEM response of a PRBS source signal*. Pure Appl. Geophys., **173**, 2777-2789.

Lien M. and Mannseth T.; 2008: *Sensitivity study of marine CSEM data for reservoir production monitoring*. Geophys., **73**, 151-163.

Liu S., Yang S., Cao Y. and Liu J.; 2010: *Analysis about response of geoelectric field parameters to water inrush volume from coal seam roof*. J. Min. Saf. Eng., **27**, 341-345.

Niu Z.L.; 2007: *Principle of time-domain electromagnetic method*. Central South University of Technology Press, Changsha, China, pp. 83-95.

Orange A., Key, K. and Constable S.; 2009: *The feasibility of reservoir monitoring using time-lapse marine CSEM*. Geophys., **74**, 21-29.

Oristaglio M.L.; 1982: *Diffusion of electromagnetic fields into the earth from a line source of current*. Geophys., **47**, 1585-1592.

Oristaglio M.L. and Hohmann G.W.; 1984: *Diffusion of electromagnetic fields into a two-dimensional earth: a finite-difference approach*. Geophys., **49**, 870-894.

Rizzo E., Suski B., Revil A., Straface S. and Troisi S.; 2004: *Self-potential signals associated with pumping tests experiments*. J. Geophys. Res.: Solid Earth, **109**, B10203, doi: 10.1029/2004JB003049.

Robinson D.A., Binley A., Crook N., Day L.F.D., Ferré T.P.A, Grauch V.J.S. and Nyquist J.; 2008: *Advancing process-based watershed hydrological research using near-surface geophysics: a vision for, and review of, electrical and magnetic geophysical methods*. Hydrol. Processes, **22**, 3604-3635.

Theis C.V.; 1935: *The relation between the lowering of the piezometric surface and the rate and duration of discharge of a well using groundwater storage*. Trans. Am. Geophys. Union, **16**, 519-524.

Titov K., Revil A., Konosavsky P. and Troisi S.; 2005: *Numerical modelling of self-potential signals associated with a pumping test experiment*. Geophys. J. R. Astron. Soc., **162**, 641-650.

Toran L., Johnson M., Nyquist J. and Rosenberry D.; 2010: *Delineating a road salt plume in lakebed sediments using electrical resistivity, piezometers, and seepage meters at Mirror Lake, New Hampshire, U.S.A*. Geophys., **75**, 73-85.

Xue G.Q., Cheng J.L., Zhou N.N., Chen W.Y. and Li H.; 2013: *Detection and monitoring of water-filled voids using transient electromagnetic method: a case study in Shanxi, China*. Environ. Earth Sci., **70**, 2263-2270.

Xue G., Hou D. and Qiu W.; 2018: *Identification of double layered water-filled zones using TEM: a case study in China*. J. Environ. Eng. Geophys., **23**, 297-304.

Yan S., Chen M.S. and Fu J.M.; 2002: *Direct time-domain numerical analysis for transient electromagnetic fields*. Chin. J. Geophys., **45**, 277-287 (in Chinese).

Yan S., Xue G.Q., Qiu W.Z., Li H. and Zhong H.S.; 2016: *Feasibility of central loop TEM method for prospecting multilayer water-filled goaf*. Appl. Geophys., **13**, 587-597.

Yang C., Liu S. and Wu R.; 2017: *Quantitative prediction of water volumes within a coal mine underlying limestone strata using geophysical methods*. Mine Water Environ., **36**, 51-58.

Corresponding author: Kang Chen
State Key Laboratory of Simulation and Regulation of Water Cycle in River Basin,
China Institute of Water Resources and Hydropower Research
A-1 Fuxing Road, Haidian District, Beijing 100038, China
Phone: +86-10-68781609; e-mail: chenkang_iwhr@126.com